

AN *IN VIVO* METHOD TO QUANTIFY BIOMECHANICAL COMPROMISE IN TENDON

R. Vanderby¹, S.E. Kuehl², M.J. Wu³, K.S. Lee⁴, and W.A. Sethares⁵

1. ABSTRACT

Computational and *in vitro* studies of tendons provide insight into functional behavior and demonstrate the intrinsic value of mechanical metrics. Methodological limitations, however, make *in vivo* data more challenging to gather and hence, rarely used clinically. Acoustoelastic (AE) analysis of ultrasound data has shown promise for providing *in vivo* mechanical data. AE studies analyze the changing ultrasound echoes in a loaded tissue and compute tissue stiffness from the AE equations. Herein, we extend these methods to tendons with local pathologies, combining AE analysis with a new method called projected empirical segmentation (PES). In cine B-mode ultrasound images, PES segments an imbedded pathological region and tracks it during functional loading. Using statistical features optimized for B-mode sonography, PES checks each pixel in a region of interest (ROI), determining whether its properties better match the interior pathological region or the exterior region of normal tissue. After objectively bounding the tendinopathy, PES segments and tracks it through subsequent cine images. The pathological tissue within this region and the normal tissue outside of this region then undergo AE analyses. Results provide localized tissue stress, strain, and stiffness from only ultrasound echo intensities. We demonstrate our method on tendinopathy regions in human Achilles tendons. Comparative local stiffnesses (normal versus tendinopathic) indicate the degree of mechanical compromise in the pathological region. Within limits of resolution and modeling assumptions, these data can quantify structural compromise and monitor functional healing in pathological tendons.

2. INTRODUCTION

Hughes and Kelly's [1] theory of acoustoelasticity (AE) describes changes in acoustic properties in a deformed medium, *e.g.* when waves travel through a medium under tensile stretch, wave velocity and reflected amplitude change. An example of this behavior in tendon (Fig. 1) shows three sets of reflected ultrasound waves from a single 2 MHz transducer superimposed to evidence AE effects for increasing tissue loads.

¹Professor, Department of Biomedical Engineering, Engineering Dr., University of Wisconsin, Madison Wisconsin 53706, USA

²Research Associate, Department of Orthopedics and Rehabilitation, University of Wisconsin, 1111 Highland Ave., Madison Wisconsin 53705, USA

³Research Assistant, Materials Science Program, University of Wisconsin, 1509 University Ave., Madison Wisconsin 53706, USA

⁴Assistant Professor, Department of Radiology, University of Wisconsin Hospital, Madison Wisconsin 53705 USA

⁵Professor, Department of Electrical and Computer Engineering, University of Wisconsin, 1415 Engineering Dr., Madison Wisconsin 53706 USA

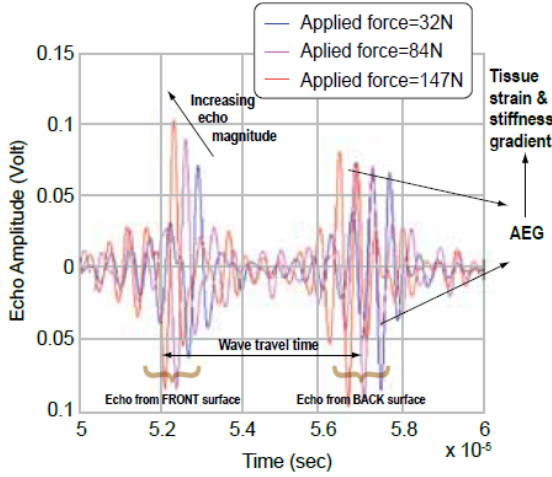


Fig. 1. Single line transducer results from an acoustoelastic test of tendon.

Note: 1) Signals from the first echo from the near surface and the second echo from the far surface are distinctive. Travel times for the waves can be accurately determined from the distance between peaks. 2) Echo amplitudes increase significantly as applied force increases. Echo changes indicate tissue stiffening.

A strong correlation between the change in wave velocity and the amount of stretch applied to tendons was reported by Crisco *et al.* [2] and Pourcelot *et al.* [3], but neither of these studies described the phenomenon within the framework of acoustoelasticity. Crevier-Denoix *et al.* [4] correlated mean echogenicity to the elastic modulus equine superficial digital flexor tendon and Pan *et al.* [5] reported an increase in echo intensity with increasing strain in skin. Neither of these phenomena were used to calculate or predict stress or strain in the tissues. De Zordo *et al.* [6] used sonoelastography (low frequency shear waves to analyze tissue vibration) to determine differences in shear stiffness (stiffer materials vibrate less) and measure softening of human extensor tendons with lateral epicondylitis. Direct measurements of tissue properties were not performed, but a comparison between healthy and pathologic tissues was included.

Since the target tissue (tendon) in Fig. 1 is subjected to axial stress (direction of tendon, x_1 , and normal to the ultrasound beam direction, x_3), the following acoustoelasticity equations can be written for each of the three directions:

$$(\tilde{C}_{11} + t_{11}) \frac{\partial^2 u_1}{\partial x_1^2} + \tilde{C}_{66} \frac{\partial^2 u_1}{\partial x_2^2} + \tilde{C}_{55} \frac{\partial^2 u_1}{\partial x_3^2} + (\tilde{C}_{12} + \tilde{C}_{66}) \frac{\partial^2 u_2}{\partial x_1 \partial x_2} + (\tilde{C}_{13} + \tilde{C}_{55}) \frac{\partial^2 u_3}{\partial x_1 \partial x_3} = \rho \frac{d^2 u_1}{dt^2} \quad (1)$$

$$(\tilde{C}_{12} + \tilde{C}_{66}) \frac{\partial^2 u_1}{\partial x_1 \partial x_2} + (\tilde{C}_{66} + t_{11}) \frac{\partial^2 u_2}{\partial x_1^2} + \tilde{C}_{22} \frac{\partial^2 u_2}{\partial x_2^2} + \tilde{C}_{44} \frac{\partial^2 u_2}{\partial x_3^2} + (\tilde{C}_{23} + \tilde{C}_{44}) \frac{\partial^2 u_3}{\partial x_2 \partial x_3} = \rho \frac{d^2 u_2}{dt^2} \quad (2)$$

$$(\tilde{C}_{13} + \tilde{C}_{55}) \frac{\partial^2 u_1}{\partial x_1 \partial x_3} + (\tilde{C}_{23} + \tilde{C}_{44}) \frac{\partial^2 u_2}{\partial x_2 \partial x_3} + (\tilde{C}_{55} + t_{11}) \frac{\partial^2 u_3}{\partial x_1^2} + \tilde{C}_{44} \frac{\partial^2 u_3}{\partial x_2^2} + \tilde{C}_{33} \frac{\partial^2 u_3}{\partial x_3^2} = \rho \frac{d^2 u_3}{dt^2} \quad (3)$$

Here, $\tilde{C}_{pq} = \tilde{C}_{pq}(\varepsilon)$ and $t_{11}(\varepsilon)$ represent the pq entries of the strain (ε) dependent stiffness matrix and Cauchy stress in the x_1 direction, respectively. Thus, reflected echo intensity, as manifested by the amplitude of the reflected ultrasound wave (Fig. 1), is altered as a tissue is loaded and relates to changes in $\tilde{C}_{33}(\varepsilon)$ if density is relatively constant. If the tissue is relatively incompressible and transverse isotropy, $\tilde{C}_{11}(\varepsilon) \propto \tilde{C}_{33}(\varepsilon)$, making strain-dependent axial stiffness $\tilde{C}_{11}(\varepsilon)$ a function of the transverse ultrasound signals. Kobayashi and Vanderby introduced a new strain energy function [7] and applied it to strain-dependent materials, computing stiffness from changes in echo intensity during deformation [8]. Duenwald *et al.* generalized this approach and applied it to the analysis of B-mode ultrasound images of porcine flexor tendons loaded *in vitro* [9].

Most current image segmentation algorithms are designed for segmenting a certain Region of Interest (ROI) from a single frame. For example, a texture discriminant is proposed for characterizing B-scans of Achilles' tendon [10], a filter algorithm is proposed for equine tendon structure identification [11], and a watershed segmentation algorithm was applied to breast tumor [12]. The active contour (snake) model [13] is an energy-minimizing spline guided by external constraints and influenced by features such as lines and edges. These image segmentation algorithms select threshold values using only features within the ROI. In contrast, the proposed Projected Empirical Segmentation (PES) algorithm operates by comparing features from within the ROI with features from a region known to be outside the ROI, allowing more advanced techniques from pattern recognition to more accurately segment.

Different frames of the video may carry different amounts of information: some frames may be blurrier than others and more difficult to segment. This paper proposes a way to segment the ROI using PES by combining two special features: projected segmentation and empirical segmentation. The projection provides automated starting points for the segmentation of the next frame and helps to prevent degradations due to the variation in image quality.

The goal of this study was: 1) Develop a computational method (PES) to segment and track tendinopathic regions as they displace and deform during functional tendon loadings and 2) integrate PES with AE analysis to obtain localized mechanical behaviors of these tissues.

3. METHODS

3.1. PES (Projected Empirical Segmentation)

We use *empirical segmentation* to generate three regions: internal, intermediate, and external to an imbedded region of tendon pathology. The internal region (user selected in the first frame) is assumed to lie well inside the final ROI (region of pathology), the external region lies outside the final ROI, and the pixels in the intermediate region must be categorized. The user specifies a seed region in the first frame, whose polygonal convex hull lies within the ROI. Two expansion ratios are applied to create two new regions: the external and the intermediate. By comparing the differences in the statistical features of the internal and external regions, an empirical value is calculated through minimum squared-error and pseudoinverse equation, as used for pattern classification [14]. The algorithm then calculates the statistical features of points in the intermediate region and compares with the empirical value to give the final ROI, which is saved for projection into the next frame. Starting with the second frame, the algorithm requires no manual intervention, since the initial region is created by combining motion estimation and the final ROI from the previous frame. The motion estimation evaluates the shift of points along frames, and the final ROI from previous frame defines the shape of the current ROI. The algorithm repeats through all remaining frames.

Then, a projection algorithm maps information from the current frame into succeeding frames, including the boundaries of the final current ROI, helping ensure that the algorithm performs well even if image quality degrades. The projection creates an initial region in the succeeding frame by combining the final ROI and the motion estimate, decreasing the time needed to compute an internal region and removing the need for the user to manually intervene in succeeding frames.

Let P_{INT} be the data set of the location of points in the internal region. Applying an expansion ratio IR creates a larger region P_A that encloses the internal region (P_{INT}). The intermediate region P_{MID} is given by:

$$P_A = IR \times P_{INT} \quad (3)$$

$$P_{MID} = [(x, y) \in P_A] \cap [(x, y) \notin P_{INT}] \quad (4)$$

The second expansion ratio ER is applied to create another region P_B that encloses both the internal region and the intermediate region. The external region P_{EXT} is given by:

$$P_B = ER \times P_{INT} \quad (5)$$

$$P_{EXT} = [(x, y) \in P_B] \cap [(x, y) \notin P_A] \quad (6)$$

Digital image correlation (DIC) is used to isolate, track and compute features of a region of interest through frames. DIC tracks the location of data set in different frames by minimizing the feature difference of selected data sets in different frames.

Statistical features are key to the successful application of empirical segmentation since they are used to distinguish the final ROI from the external region. In the PES algorithm, the statistical features are a collection of moments, which are the combinations of the pixel intensity and different orders of distance. [15]

$$\mu_{PQ} = \sum_{y=y-2}^{y=y+2} \sum_{x=x-2}^{x=x+2} (x - \bar{x})^P (y - \bar{y})^Q f(x, y) \quad (8)$$

Suppose \bar{x} and \bar{y} define the location of a pixel, x and y are locations of surrounding pixels, and $f(x, y)$ is the intensity of point (x, y) . P and Q are the orders of distance factors. With these moments, the normalized central moments can be defined. A set of invariant moments are then derived from the second and third moments. The algorithm uses a five by five matrix centering at each pixel and calculates the seven moments. This reduces the influence of inconsistent speckles and other irregularities.

3.2 Acoustoelastography

Mechanical analysis was performed using acoustoelastography (EchoSoft™, Madison WI, USA) which is based on AE theory. We adapted this software to analyze tissue within a moving and deforming region of interest both within the segmented tendinopathy and in tissue away from the pathology. The echo intensity (average gray scale brightness in the B-mode image) and spatial location of each pixel was recorded for each frame. The overall echo intensity was averaged over regions of interest to record the echo intensity changes over time, and overall strain was calculated from pixel displacement information. Echo intensity changes during stretching were interpreted within the context of the AE equations. This provided stiffness and stress via the methods of Kobayashi and Vanderby [7,8] and Duenwald *et al.* [9].

3.3 In Vivo Experiment

Two human subjects with Achilles tendinopathy were scanned with B-mode ultrasound while their tendons were passively loaded. Images were taken under protocols approved

by our Human Subjects Committee and informed consent was obtained. The exam was performed with an iU22 ultrasound system, Philips Healthcare (Andover, MA) with a variable high-frequency high-resolution 12 MHz linear-array transducer.

4. RESULTS

Figure 2 is a result of segmenting tendinopathy from the rest of the tendon image. In Figure 2a, the bright curve on the right is the surface of calcaneus. The relatively dark elliptical region on top of calcaneus (in this image) has been diagnosed as tendinopathy. Our algorithm is applied to segment the tendon from the rest of the image with expansion ratio (ER) 2.65, and the result is as Figure 2b. PES segments the regions of tendinopathy and tracks throughout the subsequent video images. Figure 2c shows the mean stress versus nominal strain behaviors for the pathological (segmented) region (blue line and data) and for a normal region of tendon proximal to the pathology (red line and data).

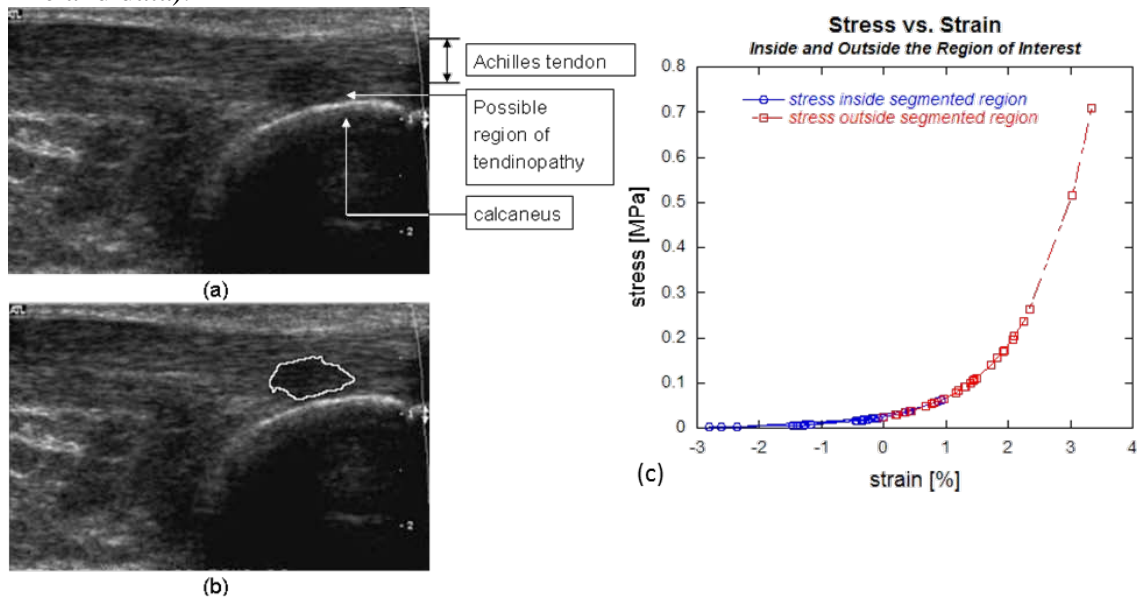


Fig. 2. a) Ultrasound image of a human Achilles tendon, b) PES segmentation to locate the tendinopathy, c) AE calculated stress in normal tissue vs. ROI as tendon is loaded

5. DISCUSSION

Tendinopathies can include regions of inflamed regions (tendinitis) and pathological region without inflammation (tendinosis). In both cases, the region is mechanically altered and compromised. Therefore, an *in vivo* mechanical evaluation would be of great value. An experienced radiologist is needed to diagnose tendonitis from ultrasound images. The PES algorithm objectively segments the region of tendonitis from the remainder of the tendon in ultrasound image. Then, subsequent AE analysis provides data lacking in any other evaluation, *i.e.* mechanical compromise of affected regions.

Compared to other clinical imaging modalities such as magnetic resonance imaging (MRI) or computed tomography (CT), ultrasound is simpler, less expensive, and more portable. This makes ultrasound an ideal tool for use for diagnosis and evaluation of tendinopathy. When used in the manner described herein, ultrasound based analyses

could quantify the initial structural compromise at presentation and track patient-specific efficacy of treatments to customize therapy.

6. ACKNOWLEDGEMENTS

This publication was made possible by Grant Number R21-EB008548 from NIBIB/NIH. EchoSoft™ software provided by Echometrix, LLC, Madison WI USA

7. REFERENCES

1. Hughes D. and Kelly J. Second-Order Elastic Deformation of Solids, *Phys. Rev.* 1953, Vol. 92, 1145–1149.
2. Crisco J. J., Dunn T. C. and McGovern R. D., Stress Wave Velocities in Bovine Patellar Tendon, *J. Biomech. Eng.*, 1998, Vol. 120, 321–326.
3. Pourcelot P., Defontaine M., Ravary B., Lematre M. and Crevier-Denoix N. A non-invasive method of tendon force measurement, *J. Biomech.*, 2005, Vol. 38, 2124–9.
4. Crevier-Denoix N., Ruel Y., Dardillat C., Jerbi H., Sanaa M., Collobert-Laugier C., Ribot X., Denoix J.-M. and Pourcelot P. Correlations between mean echogenicity and material properties of normal and diseased equine superficial digital flexor tendons: an in vitro segmental approach, *J. Biomech.*, 2005, Vol. 38, 2212–2220.
5. Pan L., Zan L. and Foster F. S. Ultrasonic and viscoelastic properties of skin under transverse mechanical stress in vitro, *Ultraso. Med. Biol.*, 1998 Vol. 24, 995–1007.
6. De Zordo T., Lill S. R., Fink C. Feuchtner G. M., Jaschke W., Bellmann-Weiler R. and Klauser A. S., Real-Time Sonoelastography of Lateral Epicondylitis: Comparison of Findings Between Patients and Healthy Volunteers, *Am. J. Roentgenol.*, 2009, Vol. 193, 180–185.
7. Kobayashi H. and Vanderby R. New Strain Energy Function for Acoustoelastic Analysis of Dilatational Waves in Nearly Incompressible, Hyper-Elastic Materials, *J. Appl. Mech.*, 2005, Vol. 72, 843–851.
8. Kobayashi H. and Vanderby R. Acoustoelastic analysis of reflected waves in nearly incompressible, hyper-elastic materials: Forward and inverse problems, *J. Acoust. Soc. Am.*, 2007, Vol. 121, 879–887.
9. Duenwald S., Kobayashi H., Frisch K., Lakes R. and Vanderby R. Ultrasound echo is related to stress and strain in tendon, *J. Biomech.*, 2011, Vol. 44, 424-429.
10. Tuthill T., Rubin J., Fowlkes J., Jamadar D. and Bude R. Frequency Analysis of Echo Texture in Tendon, *Ultrasound Med. Biol.*, 1999, Vol. 25, 959-968.
11. Meghoufel A., Cloutier G., Crevier-Denoix N., and De Guise. J. A. A thinning algorithm for equine tendon structure identification from 2D ultrasound images. *Biomedical Imaging: From Nano to Macro*, 5th IEEE International Symposium, 2008, 1565-1568.
12. Huang Y. L. and Chen D. R. Watershed Segmentation for Breast Tumor in 2-D Sonography, *Ultrasound Med. Biol.* 2004, Vol. 30, 625-632.
13. Xu C. and Prince J. Snakes, Shapes, and Gradient Vector Flow, *IEEE Transactions on Image Processing*, 1998, Vol. 7, 359-369.
14. Duda R. O., Hart P .E. and Stork D. G. *Pattern Classification*, 2nd Edition. John Wiley and Sons, 2001, 239-249.
15. Gonzales R.C. and R.E. Woods. *Digital Image Processing 2rd Edition*. Prentice Hall, 2002, 672-675.